# Transport of Stratospheric Air Masses to the Nepal Climate Observatory–Pyramid (Himalaya; 5079 m MSL): A Synoptic-Scale Investigation

A. BRACCI,*,+ P. CRISTOFANELLI,* M. SPRENGER,+ U. BONAFÈ,* F. CALZOLARI,* R. DUCHI,* P. LAJ,# A. MARINONI,* F. ROCCATO,* E. VUILLERMOZ,@ AND P. BONASONI*,@

* *Institute for Atmospheric Science and Climate, National Research Council, Bologna, Italy*
+ *Eidgenössische Technische Hochschule, Zurich, Switzerland*
# *Laboratoire de Glaciologie et Géophysique de l'Environnement, Université Grenoble 1-CNRS, Grenoble, France*
@ *EV-K2-CNR Committee, Bergamo, Italy*

(Manuscript received 26 July 2011, in final form 28 December 2011)

ABSTRACT

This work analyzes and classifies stratospheric airmass transport events (ST) detected at the Nepal Climate Observatory–Pyramid (NCO-P; 27°57′N, 86°48′E, 5079 m MSL) Global Atmospheric Watch–World Meteorological Organization station from March 2006 to February 2008. For this purpose, in situ ozone ($O_3$), meteorological parameters (atmospheric pressure and relative humidity), and black carbon (BC) are analyzed. The paper describes the synoptic-scale meteorological scenarios that are able to favor the development of ST over the southern Himalaya, by analyzing the meteorological fields provided by the ECMWF model (geopotential height, wind speed, and potential vorticity), satellite Ozone Monitoring Instrument data (total column ozone), and three-dimensional back trajectories calculated with the Lagrangian Analysis Tool (LAGRANTO) model. The study, which represents the first ''continuous'' classification of ST in the southern Himalaya, permitted classification of 94% of ST days within four synoptic-scale scenarios: stratospheric potential vorticity structures (PVS), subtropical jet stream (SJS), quasi-stationary ridges (QSR), and monsoon depressions (MD). SJS and PVS were the most frequent scenarios (48% and 30% of occurrences, respectively), QSR occurred for 12% of the ST days, and MD were detected only during the monsoon season (3%). SJS and PVS scenarios presented a peak frequency during the nonmonsoon seasons, when the jet stream and westerly disturbances influence atmospheric circulation over the southern Himalaya. During the identified ST, significant variations of $O_3$ (+24%) and BC (−56%) were recorded relative to the averaged 2-yr mean values. On average, PVS and SJS were the most effective synoptic-scale scenarios in modifying the $O_3$ and BC levels at NCO-P from postmonsoon to premonsoon seasons, and ST is one of the leading processes in defining the ''background'' BC variability at NCO-P.

## 1. Introduction

Previous studies have suggested that stratosphere–troposphere exchange (STE) is an important aspect of climate change (e.g., Sudo et al. 2003), and long-term changes in stratospheric ozone ($O_3$) input can significantly affect the tropospheric $O_3$ budget (e.g., Ordóñez et al. 2005). Tropospheric $O_3$ strongly influences the radiative budget of the atmosphere (Forster et al. 2007) and the oxidation capacity of the troposphere (Gauss et al. 2003). Today, two main inputs are recognized for tropospheric $O_3$: 1) photochemical production from nitrogen oxides coupled with decomposition of volatile organic compounds, methane, and carbon monoxide by the hydroxyl radical (e.g., Jacobson 2002) and 2) transport from the stratosphere (Wild 2007). Even if the former contribution is dominant in the troposphere, the input of $O_3$ from the stratosphere is not negligible (Lelieveld and Dentener 2000; Wild 2007). Although the total amount of $O_3$ exchanged from the stratosphere to the troposphere is basically controlled by the ''global scale'' diabatic circulation related to the downward branch of the Brewer–Dobson cell (Holton et al. 1995), smaller-scale processes occurring near the tropopause (so-called stratosphere intrusion) contribute to the irreversible transport of stratospheric air into the troposphere (ST) and strongly influence the time and space distribution of $O_3$ transport. The ST is often related to

*Corresponding author address:* P. Cristofanelli, Via Gobetti 101, 40129 Bologna, Italy.
E-mail: p.cristofanelli@isac.cnr.it

DOI: 10.1175/JAMC-D-11-0154.1

meteorological processes occurring on the synoptic scale (Holton et al. 1995). Some of the most important dynamical phenomena favoring ST are tropopause folds (Sprenger and Wernli 2003), cutoff lows (Vaughan and Price 1989; Sprenger et al. 2007; Nieto et al. 2008), and high pressure systems (e.g., Davies and Schuepbach 1994). The ST can also occur along the Arctic and subtropical jet streams (Danielsen 1968). In these regions, upper-level fronts (Keyser and Shapiro 1986), and jet streaks (i.e., wind speed maxima situated along the axis of a jet stream; Palmen and Newton 1969) can favor STE as a result of ageostrophic vertical motions and/or increased wind shear and clear-air turbulence (Traub and Lelieveld 2003).

A correct evaluation of the processes able to influence the tropospheric $O_3$ budget is an important issue especially for South Asia, given the area's sensitivity to climate change and the strong increase in anthropogenic emissions (Ramanathan et al. 2008). In particular, because of the export of pollution from the ''atmospheric brown cloud'' [ABC; i.e., the wide polluted tropospheric layers characterized by anthropogenic aerosol optical depth (AOD) greater than 0.3 and by absorbing AOD greater than 0.03, as defined by Ramanathan et al. (2007)] and from mountain valleys, the Himalaya appears to be a very critical mountain area in terms of anthropogenic impacts on air quality and regional climate (Panday and Prinn 2009; Bonasoni et al. 2010). As shown by Marinoni et al. (2010), high pollution levels, with black carbon (BC) up to 5 $\mu$g m$^{-3}$, were reached during some acute pollution episodes in the high Khumbu Valley below Mount Everest. Other than possible implications on air quality and ecosystem integrity, this pollution export plays an important climatic role. In fact, BC is an efficient absorber in UV and visible wavelengths, thus having a direct radiative effect on the energy budget of the atmosphere (Ramanathan and Carmichael 2008). Besides directly modifying the radiative equilibrium of the atmosphere, BC can also influence cloud albedo by enhancing solar radiation absorption by droplets and ice crystals. Moreover, recent studies point out that BC transport and deposition significantly affect the cryosphere (Flanner et al. 2009): BC deposition can perturb the surface energy budget of Arctic and Himalayan glaciers (Menon et al. 2010; Kopacz et al. 2011; Flanner et al. 2009, and references therein), thus implying significant changes in glacier shrinking, snow aging, and seasonal snow melting (e.g., Yasunari et al. 2010). Stratospheric air masses descending to the troposphere usually lead to airmass ''cleansing'' (see, e.g., Trickl et al. 2010) as strong gradients of anthropogenic pollutants (e.g., carbon monoxide or BC) exist between the stratosphere and the lowest/middle troposphere (e.g., Schwarz et al. 2006; Palazzi et al. 2009). Thus, ST can also contribute to determining the variability of pollutant and climate-altering anthropogenic compounds.

At the Nepal Climate Observatory–Pyramid (NCO-P; 5079 m MSL) Global Atmosphere Watch–World Meteorological Organization (GAW–WMO) station, since March of 2006, continuous measurements of trace gases, aerosol, and meteorological parameters have been conducted in the framework of the United Nations Environment Programme Atmospheric Brown Clouds project and the ''Ev-K2-CNR'' Stations at High Altitude for Research on the Environment (SHARE) project. To attain a better understanding of the $O_3$ budget in the southern Himalaya middle troposphere, Cristofanelli et al. (2009, 2010) systematically evaluated the role of the episodic downward transport of stratospheric air masses relatively deep into the troposphere in determining the observed $O_3$ variability. In particular, Cristofanelli et al. (2010) identified the days that are possibly influenced by deep ST during the March 2006–February 2008 period. A Lagrangian selection method that is based on the analysis of in situ data [$O_3$, atmospheric pressure (AP), and relative humidity (RH)], satellite total ozone values [total column ozone (TCO)], and potential vorticity (PV) along three-dimensional airmass back trajectories was adopted to identify ST to NCO-P. In particular, a specific day was considered as being influenced by ST if enhanced daily $O_3$ mixing ratio was found and at least one of the following criteria was fulfilled: 1) significant variations of daily AP value with the presence of back trajectories with PV $>$ 1.6 pvu (1 pvu $= 10^{-6}$ m$^2$ K kg$^{-1}$ s$^{-1}$); 2) presence of back trajectories with PV $>$ 1.6 pvu with significant TCO daily value increases; 3) significant variations of daily AP values with significant TCO daily value increases; 4) presence of RH $< 60\%$ with significant negative correlation of $O_3$–RH, daily $O_3$ maximum higher than the seasonal value, and significant variation of daily AP, PV, or TCO values. On the basis of this screening, 14.1% (98 days) of the investigated period was likely to be affected by ST, with an average 27.1% increase of surface $O_3$ relative to seasonal averages.

The aim of this study is to identify the most frequent synoptic-scale meteorological scenarios associated with ST observed at the NCO-P by continuous in situ measurements and to evaluate their role in determining the variability of two important climate forcers: $O_3$ and BC. To our knowledge, this represents the first systematic classification of ST in the Himalaya area. To give an indication about the relative role of each scenario in determining deep ST, we also studied the seasonal variability of the four ST scenarios. With the purpose of providing ''textbook'' examples of the synoptic-scale meteorological conditions connected with deep ST to the southern Himalaya, four

representative case studies are presented and analyzed. We calculated the average surface $O_3$ and BC variations related to the identified ST scenarios to better understand the role of ST in influencing the tropospheric composition over the southern Himalaya and to provide an improved explanation of the variability of these important climate-altering compounds.

## 2. Methods

### a. Experimental

The NCO-P (27°57′N, 86°48′E), located at 5079 m MSL in the southern Himalaya, is the highest GAW–WMO measurement station in the world. Even if at this measurement site the airmass circulation is strongly influenced by the local mountain-breeze regime, synoptic-scale circulation can effectively affect the behaviors of the atmospheric compounds (Bonasoni et al. 2010). Continuous surface $O_3$ measurements are performed with a UV-photometric analyzer (Thermo Scientific, Inc., model TEI 49C) by adopting the sampling procedures suggested within the GAW–WMO (GAW 1992) and with a combined standard uncertainty lower than ±1.5 ppbv in the range 0–100 ppbv. At the NCO-P, equivalent BC concentrations are determined using a multiangle absorption photometer (MAAP 5012 from Thermo Electron Corporation) that measures the aerosol absorption coefficient at 635 nm. For more details about BC measurements and typical behaviors at the NCO-P, please refer to Marinoni et al. (2010). Moreover, conventional meteorological parameters are continuously recorded by means of an integrated weather station (Vaisala, Inc., WXT-510). All of the in situ parameters presented in this paper are reported at local time [Nepal standard time (NPT), i.e., UTC + 5.45 h], and all concentrations refer to STP conditions. For further details on the experimental setup, please refer to Bonasoni et al. (2010).

### b. LAGRANTO model

To determine the origin of air masses reaching the NCO-P, 5-day back trajectories starting at the NCO-P were calculated every 6 h (at 0000, 0600, 1200, and 1800 UTC) with the Lagrangian Analysis Tool (LAGRANTO; Wernli and Davies 1997). To minimize possible effects of the differences between model and real topography, the 3D trajectories were started at the pressure level of 530 hPa, which almost corresponds to the station height above sea level. Trajectory calculations are based on the 6-hourly meteorological 3D gridded field composing the operational analysis produced by the European Centre for Medium-Range Weather Forecasts (ECMWF). Prior to back-trajectory calculations, the 3D ECMWF fields are interpolated onto a horizontal 1° × 1° grid. These interpolated winds, given on the original ECMWF hybrid vertical grid, are the basis for the calculation of the backward trajectories. Subgrid-scale processes like convection and turbulent diffusion are not represented in LAGRANTO back trajectories. To partially compensate for these uncertainties and also to evaluate the coherence of the flow, which depends strongly on the 3D flow structure and temporal evolution, 6 additional back trajectories with endpoints shifted by ±1° in latitude/longitude and ±50 hPa in pressure were also considered, in addition to the backward trajectory starting at the NCO-P location. For every point along the trajectory (interpolated to a time resolution of 2 h), the model provides the geographic location and altitude of the air parcel as well as other important physical quantities, such as Ertel's PV, which can facilitate the identification of stratospheric air masses at the measurement site. In fact, PV is characterized by high values (greater than 1.5–2.0 pvu) in the stratosphere, and the increase in PV values in the troposphere has been used by several authors to diagnose stratosphere-to-troposphere transport events (e.g., Schuepbach et al. 1999). In the absence of diabatic heating or frictional forces, PV is a conserved quantity defined by

$$\mathrm{PV} = -g\frac{d\theta}{dp}(\varepsilon + f),$$

where $g$ is the gravitational acceleration, $\theta$ is potential temperature, $p$ is pressure, $\varepsilon$ is the component of the curl of wind vector normal to an isentropic surface, and $f$ is the Coriolis parameter.

### c. Synoptic-scale ST diagnostic

The synoptic-scale meteorological conditions related to the ST detected at the NCO-P are determined on the basis of the meteorological fields provided by ECMWF operational analyses. The data are based upon the T159L60 spectral model with a time resolution of 6 h. The spatial resolution of T159 corresponds to a spatial resolution of 1.125° × 1.125° in the geographical grid, which corresponds to about 100 km at the NCO-P. Among the 60 levels, about 19 cover the region from 100 to 600 hPa, which is the most relevant for deep ST. In particular, the synoptic-scale analysis considers the following meteorological fields: geopotential heights at different pressure levels (850, 500, and 250 hPa), wind speed at 200 hPa, isentropic PV at 330 K, and vertical cross section of PV, RH, and wind speed. It is likely that the ECMWF operational analysis provides the most accurate representation of the atmosphere in this region.

It was applied in several studies covering the Himalaya (e.g., Schiemann et al. 2009). We expect the mesoscale and synoptic scale to be well represented in the ECMWF analysis; on the other hand, smaller-scale or near-surface features, which directly relate to the complex topography in this region, are certainly not representative. These small-scale features do not restrict the validity of our study, however, which strongly focuses on large-scale processes.

Several investigations have pointed out the presence of high TCO horizontal/temporal gradients when a stratospheric air mass slanted into the troposphere (e.g., Holton et al. 1995; Goering et al. 2001; Wimmers and Moody 2004). In fact, during a cutoff low or tropopause folding, a local TCO maximum can be observed, separated from the surrounding by very steep gradients. For these reasons, TCO maps as well as daily values for the NCO-P location (pixel extension: 1.00° latitude × 1.25° longitude; local time overpass: ~1200) were analyzed, as furnished by the Dutch–Finnish Ozone Monitoring Instrument (OMI; Levelt et al. 2006a,b) on board the National Aeronautics and Space Administration (NASA) Earth Observing System *Aura* satellite (Schoeberl et al. 2006).

## 3. Results

### *a. Classification of stratospheric airmass transport at the NCO-P: Synoptic-scale scenarios*

The dynamics of ST were investigated during the period of March 2006–February 2008 at the NCO-P from the ST identification reported in Cristofanelli et al. (2010). During the considered period, 98 days (14.1% of the whole dataset) were considered as plausibly affected by ST. To classify the synoptic-scale meteorological scenarios that induced the transport of stratospheric air to the measurement site, each ST was analyzed by using the methods described in section 2. This led to the recognition of four main scenarios, conductive for ST at NCO-P and over the southern Himalaya. In particular, the presence of 1) stratospheric PV structures (PVS) associated with a meridionally perturbed jet stream, 2) an essentially zonal subtropical jet stream (SJS), 3) quasi-stationary ridges (QSR), and 4) monsoon depressions (MD) were able to explain 94% of detected ST events. Note that each ST event has been associated with only one of the scenarios. In the following list, a general description of each scenario is provided:

1) PVS—As indicated by Bohmer (2006), the Himalaya is frequently affected by westerly disturbances (i.e., atmospheric troughs or cutoff lows). The fluctuations of the westerly flow lead to the formation of successive troughs and ridges that can produce ageostrophic circulation resulting in tropopause foldings (Moore and Vanknowe 1992). Turbulent and diabatic mixing across the fold edges can cause irreversible transfer of stratospheric air masses into the troposphere (Beekmann et al. 1997), thus favoring ST. These westerly disturbances can eventually evolve in a cutoff low, where ST can be caused by convective or radiative erosion of the tropopause and turbulent mixing inside the cyclonic vortex (Vaughan and Price 1989). Moreover, the breakup of stratospheric streamers can further favor the occurrence of ST (Appenzeller et al. 1996). These westerly disturbances are often related to enhanced nonzonal jet streams with PVS. According to Hoskins et al. (1985), the term ''PV structures'' refers to isentropic PV streamers and cutoff lows in the upper troposphere/lower stratosphere. In particular, stratospheric PV streamers are narrow filaments of high-PV air extending toward the equator and eventually breaking up in a distinct cut off (Sprenger et al. 2007; Nieto et al. 2008). As indicated by Sprenger et al. (2007), PVS and ST are closely correlated: on isentropes below 320 K, 30%–50% of PVS are associated with ST.
2) SJS—Well-defined zonal SJS can trigger STE over South Asia and the Tibetan Plateau (Zachariasse et al. 2000; Hitchman et al. 2004; Ding and Wang 2006). As indicated by Shapiro et al. (1987) and Hudson et al. (2003), there is a close coincidence between the SJS and the upper-level subtropical front, where shallow tropopause foldings are likely to occur (Langford 1999). Even if tropopause folding associated with SJS is usually less deep in the troposphere than that occurring along the polar jet stream, it appears to be more frequent (Sprenger et al. 2003). Exchange can also occur as a result of filamentation around the SJS, causing a quasi-horizontal stretching of stratospheric materials along isentropes (Appenzeller and Holton 1997). Clear-air turbulence in the strong shear zone near the SJS can further enhance vertical airmass mixing and ST (Zachariasse et al. 2000). Furthermore, local wind speed maxima embedded in the jet streams are favorable places for ST. Indeed, these so-called jet streaks are associated with ageostrophic vertical motions (Moore and Vanknowe 1992; Keyser and Shapiro 1986).
3) QSR—During the period of investigation, wide high pressure areas with axes north of the Himalaya were observed. In extreme cases, this QSR can evolve as an atmospheric blocking (Croci-Maspoli et al. 2007). As shown by ECMWF analyses, in such situations the NCO-P is usually located at the southeastern border of the typical Ω-shaped area of the QSR, in the left entrance region of the SJS, where downward

motions are expected. As shown by Mohanakumar (2008), high pressure areas related to blocking systems can effectively modify the horizontal and vertical airmass transport and, hence, the distribution of trace substances in the troposphere and lowest stratosphere. In particular, the mixing of stratospheric air into the troposphere can occur at the western and eastern boundary of the blocking system, where a very low tropopause (occasionally close to the 5000-hPa pressure level) can occur (Ebel et al. 2008). Moreover, according to Davies and Schuepbach (1994) and following the classical STE picture of Danielsen (1968), the anticyclonic subsidence may transport downward the ozone-rich stratospheric air that intrudes into the upper/middle troposphere. Note that the QSR can be seen as negative PV anomalies, often related to the occurrence of leading or trailing PVS [see, e.g., section 3b(3)]. However, we decided to separate the QSR from the PVS cases because, as suggested from the analyses of the case studies, it appears likely that the subsidence related to the high pressure system can play an important role in steering the stratospheric air masses down to the measurement site.

4) MD—During the summer monsoon, deep low pressure systems can be observed over the Bay of Bengal (Barros and Lang 2003). The easterly jet over Southeast Asia enables the depressions over the Bay of Bengal to penetrate into the Indian plain toward the southern Himalaya. As shown by Loring et al. (1996) and Das (2009), STE can occur in the vicinity of midlatitude or tropical cyclones. Kumar (2006) pointed out that overshooting convection above the Indian Peninsula during the summer monsoon can lead to a weaker temperature vertical gradient and enhanced mass flux across the tropopause, with strong downdrafts in the vicinity of the tropopause during the decaying stage of the convective system. Thus, as is also shown in the following case study, during their northward motion across the Indian plains, the MDs can promote strong vertical motions, possibly favoring ST at the NCO-P.

The frequency of the identified synoptic scenarios was analyzed in terms of seasonal occurrences (Table 1), following the season definition reported in Bonasoni et al. (2010) for the NCO-P region: winter, premonsoon, monsoon, and postmonsoon. Over the 2-yr period, the PVS and SJS scenarios were the most frequent (30.2% and 47.9% of ST days, respectively), while the MD class (3.1%) occurred only during the monsoon season. For the remaining ST days (6.2%) it was not possible to unambiguously attribute a synoptic-scale scenario that was conducive for ST, and thus they were unclassified (UN). The SJS scenarios predominantly occurred (26.0% of analyzed days) during winter, when the subtropical upper front is almost permanently located over the Himalayan Ridge, and the PVS scenario was most frequent during the premonsoon (14.6% of analyzed days), when westerly disturbances (upper-level troughs and cutoff lows) and embedded jet streams often affect the southern Himalaya (Bohmer 2006). These results are in agreement with the climatological description of the westerly jet position over the Tibetan Plateau reported by Schiemann et al. (2009). In fact, during winter a strong and narrow zonal jet is exactly located over the Himalaya (with axis at 28°N). During the premonsoon, the jet shows the same average position but with an increased dispersion over a wide range of latitudes, supporting meridional excursion related to synoptic-scale variability. During summer monsoon, the jet axis is located northward of the Tibetan Plateau and weakens considerably. During postmonsoon, the jet moves and intensifies again toward the Himalaya, showing a smaller meridional dispersion than during the premonsoon. As indicated by the analyses of the detected events, STE processes occurring very far upwind (i.e., more than 5 days before the detection of stratospheric air masses over the southern Himalaya) were still detectable at NCO-P. This is in agreement with the previous work by Zachariasse et al. (2000), who found, for the subtropical Indian Ocean, layers of stratospheric air masses rich in $O_3$ transported over thousands of kilometers after tropopause crossing. Also in agreement with the recent findings by Trickl et al. (2011), this appeared to be the case for 33% of SJS days, which were traced back to STE occurring along the North Africa/Arabian jet, over the Mediterranean Basin, or over even more westerly regions (e.g., Atlantic Ocean), thus indicating that distant STE can still influence airmass composition over the southern Himalaya. QSR scenarios were only observed during the premonsoon (frequency: 7.3%) and postmonsoon (5.2%). During the monsoon season, the few stratospheric intrusions detected (3 days) were exclusively related to the presence of MD over the Bay of Bengal moving toward the Indian plains.

TABLE 1. Seasonal ST frequency at NCO-P for the different synoptic scenarios defined in section 3 over March 2006–February 2008.

| Seasons | ST days | PVS | SJS | QSR | MD | UN |
|---|---|---|---|---|---|---|
| Premonsoon | 43 | 14.6% | 17.7% | 7.3% | — | 4.2% |
| Monsoon | 3 | — | — | — | 3.1% | — |
| Postmonsoon | 15 | 5.2% | 4.2% | 5.2% | — | 1.0% |
| Winter | 37 | 10.4% | 26.0% | — | — | 1.0% |
| Total | 98 | 30.2% | 47.9% | 12.5% | 3.1% | 6.2% |

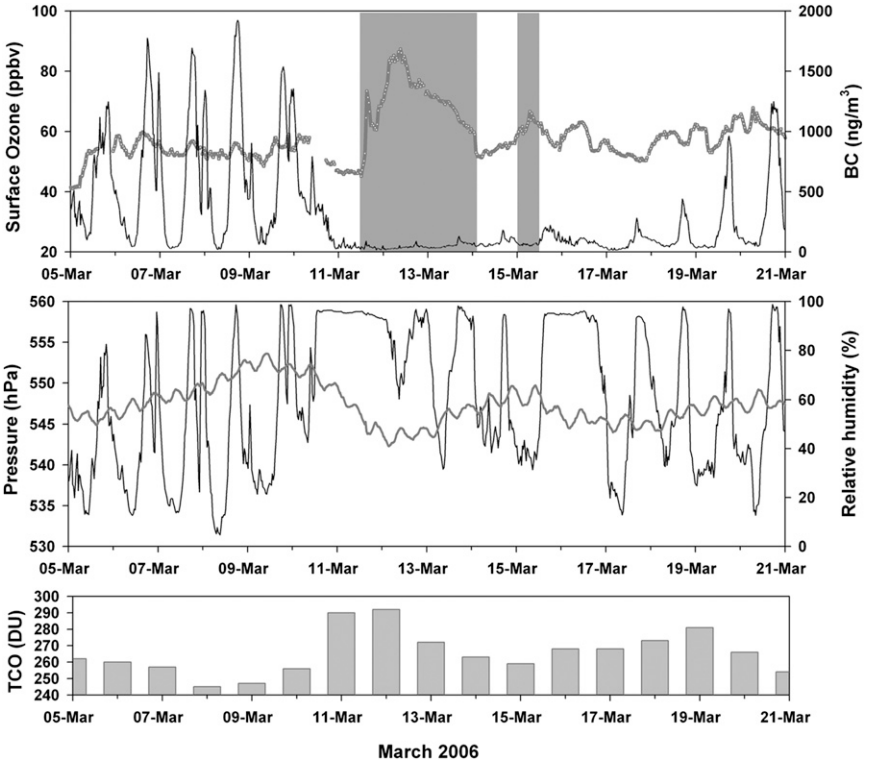


FIG. 1. (top) Surface $O_3$ and BC, (middle) atmospheric pressure (gray line) and relative humidity (black line), and (bottom) TCO at NCO-P from 5 to 21 Mar 2006. The vertical gray bars denote the periods affected by ST as defined by Cristofanelli et al. (2010).

### *b. Textbook examples of stratospheric intrusion at NCO-P*

#### 1) STRATOSPHERIC PV STRUCTURES: 11–13 MARCH 2006

As showed by Bonasoni et al. (2010), a strong correlation characterized $O_3$ and BC variations at NCO-P on a daily basis, especially during nonmonsoon seasons. As already reported by Bonasoni et al. (2010) and Marinoni et al. (2010), the diurnal variability of $O_3$ and BC is likely related to the transport of polluted air masses from the lower troposphere by daytime thermal wind, as testified to by the strong correlation with specific humidity, RH, and local wind regime variability. This was evident also for the period 5–21 March 2006, when high $O_3$, BC, and RH values usually characterized the measurement site during daytime, when up-valley winds transported more-humid air masses from lower altitudes up to NCO-P (Fig. 1). Starting at 1200 NPT 11 March 2006, within 20 h, 30-min average $O_3$ concentrations increased from 46 to 87 ppbv (at 0900 NPT 12 March 2006; see Fig. 1), a value that is significantly above the monthly-mean average (59 ppbv, over two years). A strong pressure minimum (543 hPa) was recorded almost simultaneously with the highest $O_3$ values, suggesting a possible relationship between the high $O_3$ levels and the trough passage (Fig. 1). Of interest is that very low BC levels (37 ng $m^{-3}$) were recorded until 16 March 2006. These values were about an order of magnitude less than the average monthly value (459 ng $m^{-3}$), thus indicating the presence of very clean air masses at the measurement site. Relative humidity values above 90% were continuously recorded for 36 h before the event, and during the $O_3$ peak RH decreased to 60%, indicating the presence of a drier air mass at the measurement site.

As shown by the ECMWF analyses (Fig. 2), starting from 10 March 2006 a trough affected the Indian subcontinent and Himalayan region while high values of 200-hPa wind speed (higher than 45 m $s^{-1}$) were observed south of the Tibetan Plateau. As deduced by analysis of air temperature at 500 hPa (not shown), the trough was characterized by being colder than the surrounding regions. Dry air is embedded within the trough core while a narrow band with high RH values was present on the eastern flank of the trough. High RH values were also present along the southern Himalaya and at NCO-P (see Fig. 2) because of the northward advection of air masses within the warm sector. The

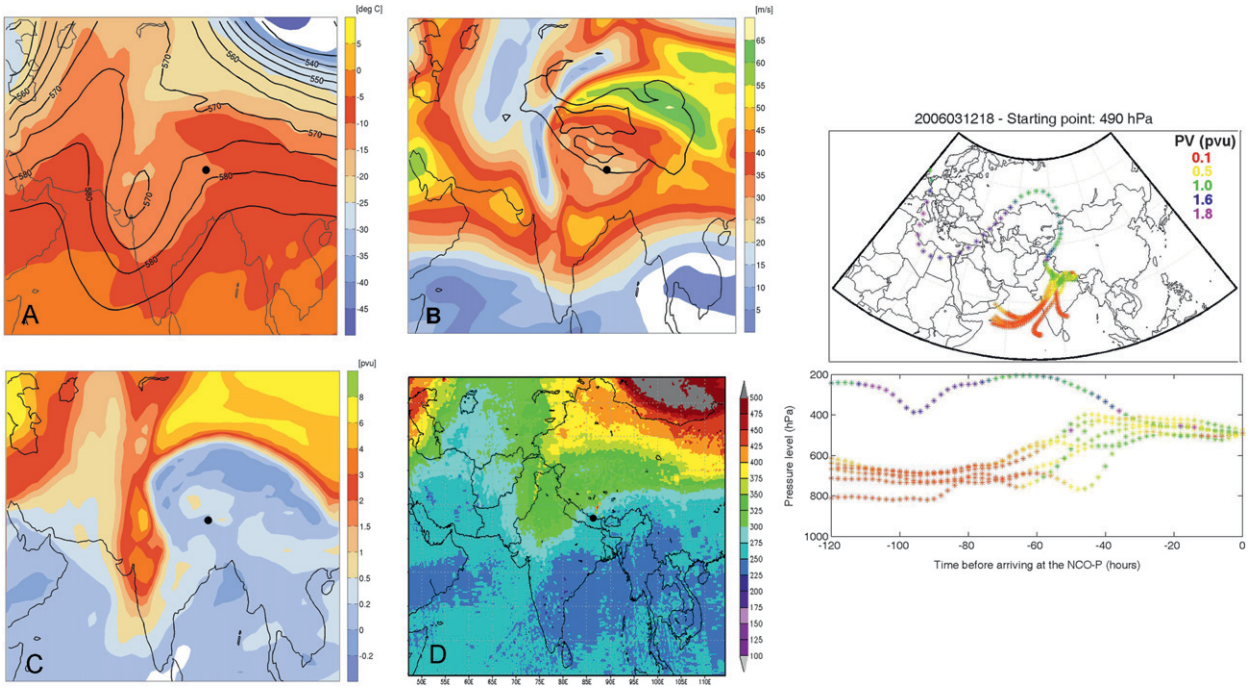


FIG. 2. (a) ECMWF geopotential height (isolines; gpdam) and air-temperature contours (colored scale) at 500 hPa, (b) wind speed at 200 hPa, (c) ECMWF PV at the 330-K surface, and (d) OMI TCO field (DU) for 1200 UTC (1745 NPT) 10 Mar 2006. In (b) the 700- and 550-hPa isolines of surface pressure are included to provide a representation of the topography. (right) Backward-trajectory ensemble arriving at NCO-P with color code representing PV values reported for 1800 UTC (2345 NPT) 12 Mar 2006.

trough, with axis from southwest to northeast, was moving eastward in the following days, reaching NCO-P between 11 and 12 March 2006. It disappeared on 13 March 2006. As reported by the analysis of PV at the 330-K surface, on 10 March a streamer characterized by high PV values (>2 pvu) was associated with the observed trough and extended from the Tibetan Plateau to the Indian plain (Fig. 2). On the following day, the PV streamer broke up into a distinct PV cutoff, which passed over NCO-P at 0600 UTC 12 March—that is, at the time of the observed $O_3$ maximum and AP minimum. As shown by Sprenger et al. (2007), this is a strong indication of stratosphere-to-troposphere airmass transport. To describe further the synoptic-scale scenarios leading to the observed ST, the TCO horizontal field deduced by the OMI measurement was analyzed. Figure 2 shows a tongue of relatively high TCO values [>300 Dobson units (DU); one Dobson unit refers to a layer of gas that would be 10 $\mu$m thick under standard temperature and pressure] overlapping the PV streamer and affecting the Himalayan Ridge. In particular, as seen in Fig. 1, large variations of TCO were recorded over NCO-P between 10 and 13 March (290 DU). Several investigations have found that the presence of high TCO horizontal/temporal gradients can reveal the intrusion of a slanting stratospheric air mass into the troposphere (e.g., Holton et al. 1995; Goering et al. 2001). In particular, on 12 March 2006, the PV and potential temperature meridional cross sections obtained from ECMWF analyses confirmed the presence of a tropopause fold slanting from the stratospheric reservoir down to 380 hPa from 35° to 25°N (Fig. 3a). Even if the "core" of this folding did not directly affect the NCO-P location, a tongue of relatively dry (RH of ~50%) air masses rich in PV (>1 pvu) brushed the southern slope of the Himalaya (Fig. 3b). These analyses suggested that the cutoff low could promote STE over the Himalaya, even if smaller-scale processes (not recognized by the ECMWF data) were likely to further favor the transport of stratospheric air masses to NCO-P. The analysis of LAGRANTO 3D back trajectories showed a complex situation for this case study. As an example, Fig. 2 shows the 490-hPa back-trajectory ensemble ending at NCO-P at 1800 UTC 12 March 2006: only 1/7 of the back trajectories showed stratospheric PV values (i.e., PV > 1.6 pvu) along its path over central Asia.

### 2) SUBTROPICAL JET STREAM: 13–18 JANUARY 2007

From 13 to 18 January 2007, several $O_3$ peaks were recorded at NCO-P (Fig. 4). In general, evident diurnal variations for BC and RH have been observed also for this period. This is in agreement with the occurrence of

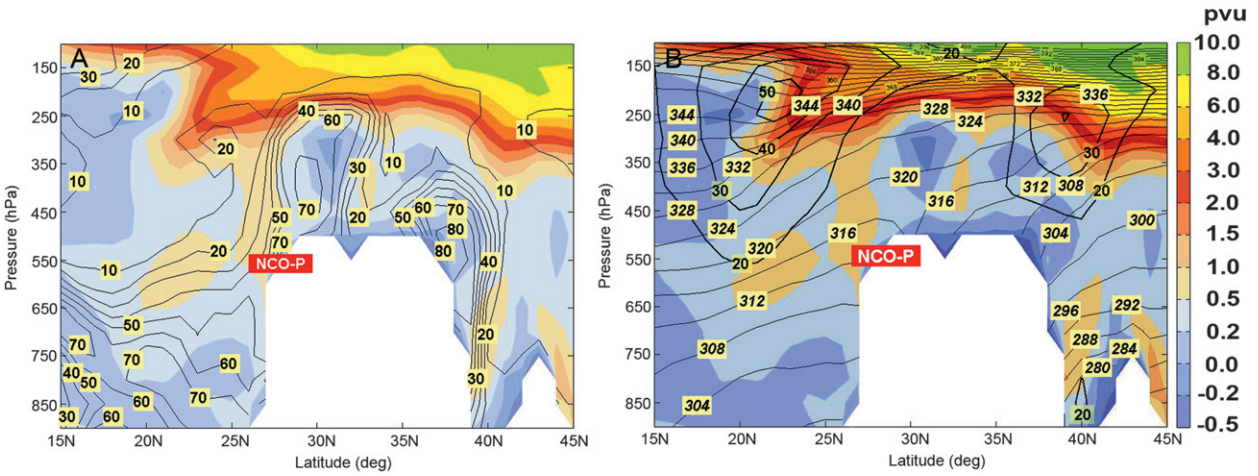


FIG. 3. At 0600 UTC (1145 NPT) 12 Mar 2006: vertical cross section of PV (colored scale) with (a) isolines of RH (%) and (b) jet speed (thick lines; m $s^{-1}$) and potential temperature (thin lines with italic labels; K).

polluted (and moister) airmass transport from the lower troposphere because of thermal wind circulation over the southern Himalayan foothills as described by Bonasoni et al. (2010) and Marinoni et al. (2010). As shown below, the peaks were probably connected with a well-defined SJS over the southern Himalaya. During this period, the surface pressure showed a decreasing trend, reaching a minimum on 15 January 2007 (540 hPa), thus suggesting a possible relationship with the $O_3$ peaks observed on 14 January (53 ppbv), 16–17 January (57 ppbv), and 18 January (55 ppbv). Simultaneous with the $O_3$ increases, low BC levels (average value: 78 ± 37 ng $m^{-3}$) were observed at the measurement site, indicating the presence of clean, dry (RH < 25%) air masses. During

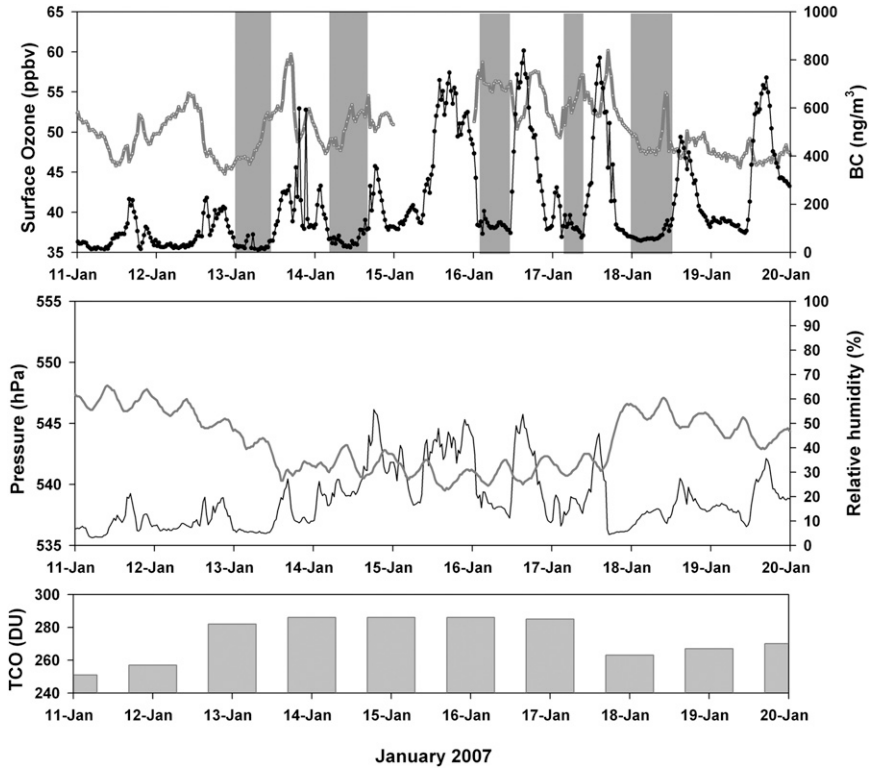


FIG. 4. As in Fig. 1, but from 11 to 20 Jan 2007.

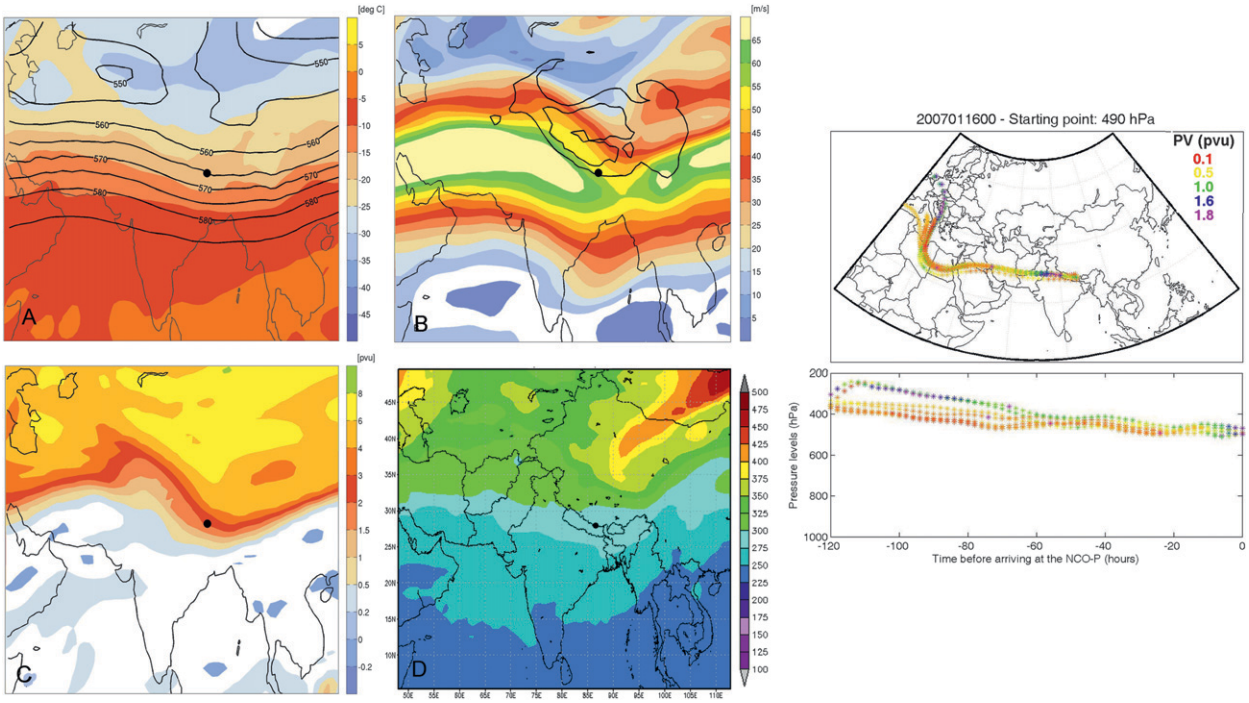


FIG. 5. As in Fig. 2, but (a)–(d) for 0000 UTC (0545 NPT) 14 Jan 2007 and (right) for 0000 UTC (0545 NPT) 16 Jan 2007.

the afternoon periods, higher BC values characterized NCO-P because of the valley-wind regime transporting more-polluted air masses from the lower troposphere to the high Khumbu Valley (Bonasoni et al. 2010; Marinoni et al. 2010). This finding underlines the importance of analyzing continuous high-frequency data for correctly evaluating the contribution of different airmass transport processes in such complex topography. As shown by the ECMWF analysis at 500 hPa (Fig. 5), South Asia and the Himalaya were characterized by the presence of a strong meridional geopotential gradient, indicating the upper-level subtropical front (Hudson et al. 2003). The wind speed analysis at 200 hPa suggested the presence of the SJS in the same region. The PV field at 330 K was mainly characterized by a zonal symmetry, although some fluctuations were evident on 14 January (Fig. 5), with a PV value of 2 pvu near the southern Himalaya. As deduced from OMI data (Fig. 4), during this period the southern Himalaya and NCO-P were characterized by an increase in TCO (+35 DU from 11 January) and were located within a high TCO gradient that, according to Hudson et al. (2003), separates the midlatitudes from the subtropical TCO regime (Fig. 5). The vertical cross section of PV, wind speed, and RH showed a tongue of relatively high PV and dry air masses in the northern flank of the jet core over the southern Himalaya (Fig. 6). An evident tilting of isentropes was also present over NCO-P (Fig. 6b), indicating that the isentropic transport of stratospheric air masses was likely in this case. To evaluate the possible role of turbulence in favoring the descent of stratospheric air masses to NCO-P, the turbulence index (TI) as defined by Ellrod and Knapp (1992) was calculated (not shown here). High values of TI (higher than $22 \times 10^{-7}$ s$^{-2}$) were present on the southern slope of the Himalaya below the jet core. This high turbulent zone could have contributed to the downward transport to the measurement site (Traub and Lelieveld 2003; Ding and Wang 2006).

The analysis of LAGRANTO back-trajectory ensembles (Fig. 5) allowed a better analysis of the atmospheric transport that air masses could have experienced toward the measurement site. For the sake of simplicity, only the back trajectories ending at NCO-P at 0545 NPT (0000 UTC) 16 January 2007 are described here. On the horizontal projection, the trajectories perfectly followed the shape of the SJS over North Africa and central Asia, with descending motions from above 400 hPa. The $^3/_7$ back trajectories composing the ensemble showed PV greater than 1.6 pvu, thus indicating contact with stratospheric air masses. In agreement with the PV vertical cross section (Fig. 6), the back trajectories were characterized by PV values ranging from 1.0 to 1.6 pvu just upwind of the measurement site, supporting the hypothesis of "local" STE occurring right over the Himalayan Ridge. Moreover, the LAGRANTO back trajectories indicated that stratospheric inputs were also likely far upstream of the measurement site, as shown by

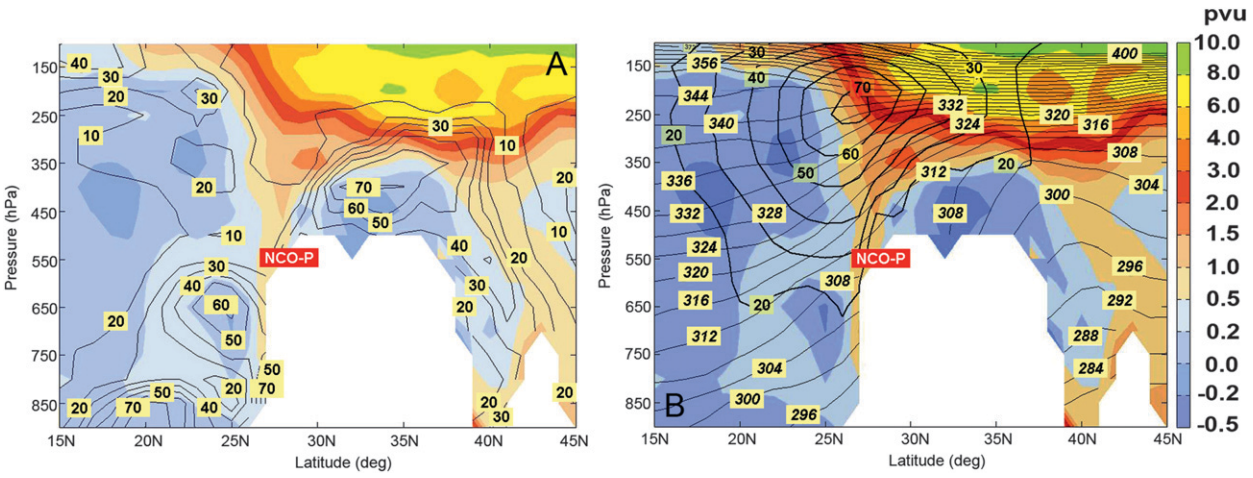


FIG. 6. As in Fig. 3, but at 1800 UTC (2345 NPT) 15 Jan 2007.

the high PV values observed over southern Europe 5 days before the air mass arrived at NCO-P. Such high PV values could be related to ST occurring in connection with an upper-air front (not shown here). Thus, in some cases, the stratospheric air masses detected at NCO-P could also originate from STE occurring very far upstream of the southern Himalaya.

### 3) QUASI-STATIONARY RIDGE: 27–28 APRIL 2006

At NCO-P the last days of April 2006 (from 27 to 28 April) were characterized by a rising of surface pressure (peak value: 553 hPa at 0945 NPT 28 April), low values of RH (down to 20% at 1100 NPT 27 April and from 0330 to 1530 NPT 28 April), and low BC (average value: $105 \pm 30$ ng m$^{-3}$). Starting from the late afternoon on 27 April, a steady increase in surface $O_3$ was recorded, with a peak of 78 ppbv at 2145 NPT and a second maximum (88 ppbv) at 1515 NPT 28 April (Fig. 7).

As suggested by the analyses of geopotential height and air temperature at 500 hPa (not shown), on 24 April 2006, a trough stretched from western Russia to the Black Sea and eastern Mediterranean Sea. During the following days this trough moved southeastward, and on 26 April it elongated over Arabian Peninsula. This trough represents the west wing of a high pressure ridge with axis elongating from northwest to southeast over Uzbekistan and Afghanistan. In the following days, the high pressure ridge reinforced and its axis slightly rotated to north–south. As deduced by the ECMWF geopotential height analysis at 500 hPa, from 27 to 28 August 2006, the Tibetan Plateau and the southern Himalaya were under the influence of this high pressure ridge (Fig. 8), which also favored the pressure increase observed at the measurement site. As a consequence, the SJS was confined to high latitudes, with weaker wind over the Tibetan Plateau and Himalaya, as indicated by the wind speed analysis at 200 hPa (Fig. 8). The PV and TCO fields accurately reproduced the shape of the ridge, with lower values in the core of the high pressure system and a significant gradient along the ridge boundaries (Fig. 8). Under this scenario, the NCO-P was located at the southeastern edge of the classic Ω ridge shape, where a PV streamer was also present. The analysis of the vertical PV cross section showed a tropopause fold over the Himalaya with a tongue of elevated PV (Fig. 9) slanting southward to about 400 hPa over NCO-P. The analysis of the local wind behavior at NCO-P from 1945 NPT 26 April to 1545 NPT 28 April (wind steadiness: 0.92) evidenced that a mountain-breeze flow continuously affected the Khumbu Valley. This is a signal of strong synoptic-scale forcing also on the local/regional scale. In fact, as reported by Bonasoni et al. (2010), the absence of the typical daytime up-valley wind usually characterizing the upper Khumbu Valley is a clear indication of synoptic forcing to the regional circulation, which could have favored the downward motions of air masses to NCO-P. A further contribution of stratospheric air masses is suggested by LAGRANTO analysis (Fig. 8). Even if PV never exceeds 1.6 pvu during the airmass travel, at 0000 UTC (0545 NPT) 28 April just before the observed $O_3$ peak, the air masses arriving at NCO-P showed coherent 80-h subsidence starting from 300 to 400 hPa. As shown by Fig. 8c, such air masses could originate from a PV streamer over the Middle East, which corresponds to an upper trough (Fig. 8a) characterized by the presence of a strong TCO gradient (Fig. 8b). The PV streamer was already present in this region when the air masses reaching NCO-P passed through it (i.e., on 23 April 2006).

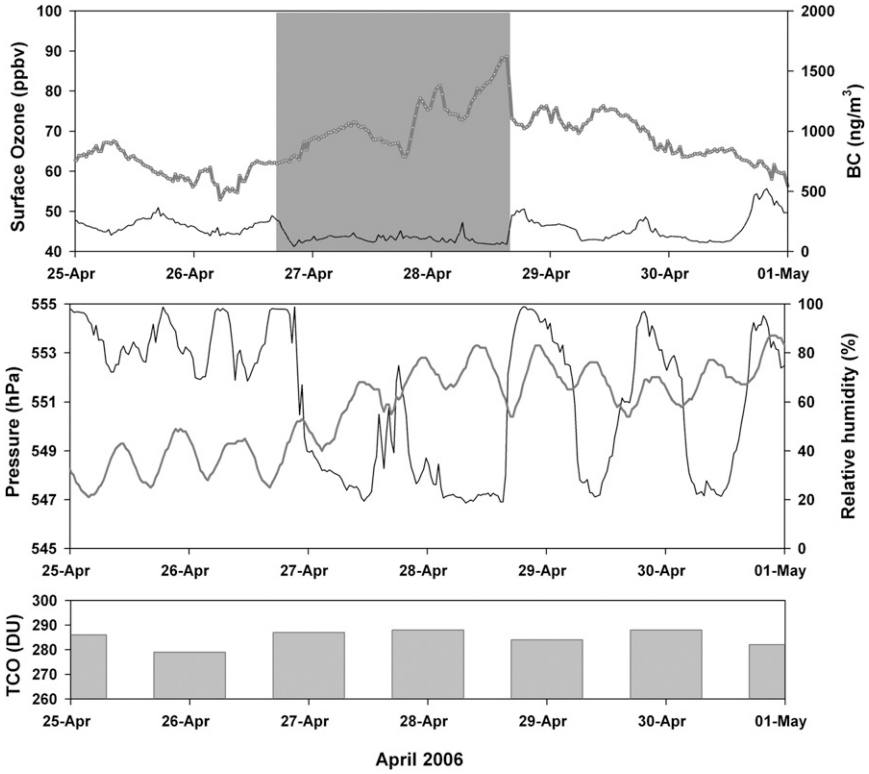


FIG. 7. As in Fig. 1, but from 25 Apr to 1 May 2006.

4) MONSOON DEPRESSION: 23 SEPTEMBER 2007

Even if the MD scenarios only accounted for 3% of the ST days observed during the investigation period, the authors evaluated whether describing a typical ST event under this scenario can provide interesting information for better characterizing ST to the Himalaya. A 12-h significant decrease in RH (down to 40%) was observed at NCO-P from 0200 to 1500 NPT 23 September 2007 (Fig. 10). At 0800 NPT 23 September, $O_3$ increased to 57 ppb, a value well above the average value for the 2007 monsoon season (37 ± 8 ppbv). Again, the low BC values (21 ng $m^{-3}$) observed at the site suggested that it was affected by clean air masses. On 22 September, relatively high TCO values (272 DU, above the 75th percentile of the 2007 monsoon values) were observed by OMI above NCO-P. Starting on the same day, AP slightly decreased, reaching the lowest value of 550 hPa on 24 September 2007: this indicated that the NCO-P area was affected by the influence of a low pressure system. In fact, the ECMWF geopotential analysis at 500 hPa (Fig. 11), showed a low pressure area over the Bay of Bengal that moved northward into the Indian plains. As shown by the wind speed analysis at 500 hPa, gale winds (up to 17.5 m $s^{-1}$) were also present in the region between NCO-P and the depression center. At lower atmospheric levels (not shown) the low pressure area was even clearer. The presence of the deep depression was also highlighted by the ECMWF analysis at the 330-K surface (Fig. 11), with PV values up to 2 pvu over the Bay of Bengal. Such high PV values were due to diabatic processes related to latent heat release and differential heating within the cyclonic region. On 22 September 2007, when the highest OMI–TCO value was observed over the NCO-P, a tongue of relatively high TCO (>275 DU) stretched along the southern ridge of the Himalaya (Fig. 11).

To obtain a better understanding of the processes leading to the presence of dry air masses rich in $O_3$ and poor in BC at NCO-P, analyses were performed of the vertical cross section of PV, potential temperature, RH, and wind speed along the transect from 15° to 45°N (Fig. 12). It was found that the jet stream was located north of the Tibetan Plateau and far away from NCO-P. The PV cross section showed that the low pressure system over the Bay of Bengal was characterized by high PV values (up to 2 pvu) up to 450 hPa, due to diabatic processes occurring within the low pressure area. For this complex case study, the ST was likely to be associated with vertical airmass exchange and/or with subsidence occurring around the periphery of the tropical cyclone. In fact, previous studies had already suggested that transient $O_3$

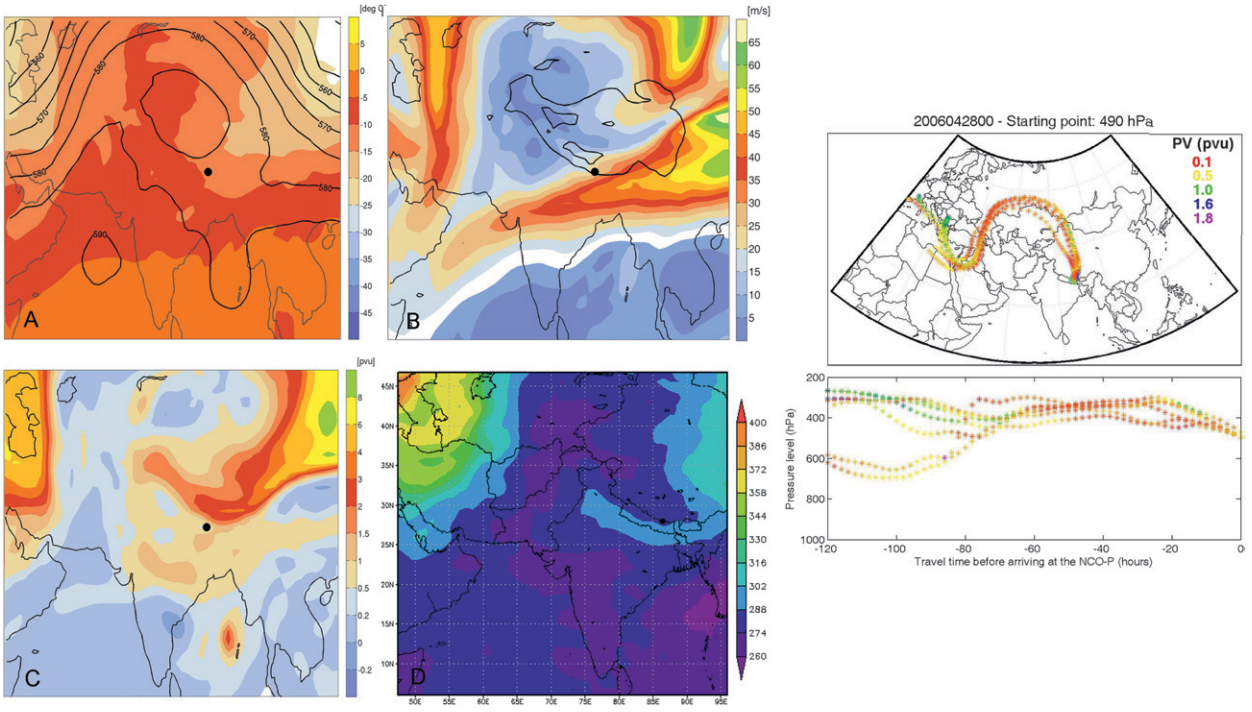


FIG. 8. As in Fig. 2, but (a)–(d) for 1800 UTC (2345 NPT) 27 Apr 2006 and (right) for 0000 UTC (0545 NPT) 28 Apr 2006.

maximum in the troposphere could be associated with STE occurring in the vicinity of midlatitude or tropical cyclones (e.g., Loring et al. 1996; Das 2009). The Moderate Resolution Imaging Spectroradiometer (MODIS) satellite-observed cloud-top temperature (version 5.1) was retrieved to infer an evaluation of the possible vertical cloud extension. Together with the low values of outgoing longwave radiation (down to 155 W $m^{-2}$, as observed by the NASA Atmospheric Infrared Sounder), the low cloud-top temperatures (down to 195 K) suggested the presence of high-altitude convective clouds over the cyclonic area, which can favor vertical airmass exchange and STE (e.g., Kumar 2006). As shown by LAGRANTO back trajectories (Fig. 11), easterly air masses reached NCO-P as a result of the presence of the depression. In particular, the site was located at the borderline between flows coming from the core of the low pressure system and the north Tibetan Plateau. The majority (5/7) of these back trajectories ending at the measurement site at 0600 UTC (1145 NPT)

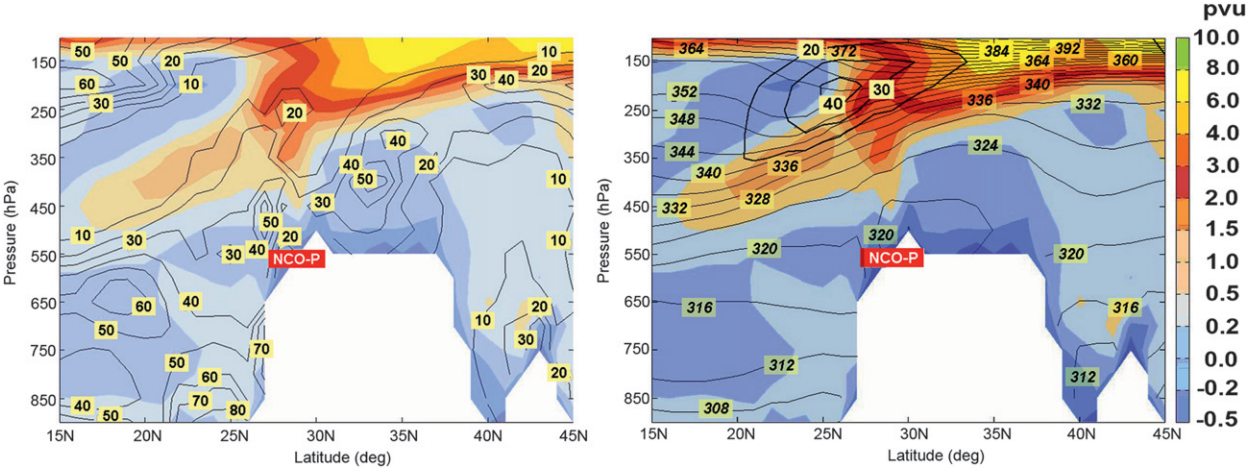


FIG. 9. As in Fig. 3, but at 0600 UTC (1145 NPT) 28 Apr 2006.

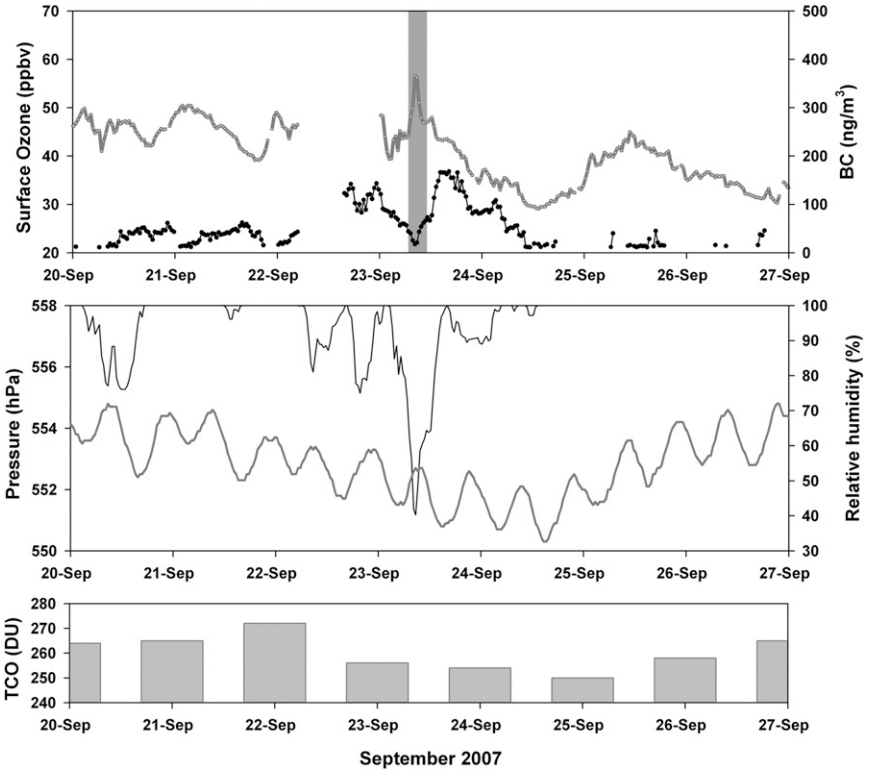


FIG. 10. As in Fig. 1, but from 20 to 27 Sep 2007.

23 September 2007 (i.e., approximately at the time of $O_3$ peak) were related to descending clockwise circulation and subsidence, favoring the arrival at the measurement site of air masses with relatively high PV values (3/5 back trajectories showing PV values above 1.6 pvu).

The analysis of the RH cross section (Fig. 12a) suggested the presence of downward dry air masses (RH less than 60%) at the northern border of the cyclonic area, also affecting the southern slope of the Himalaya where NCO-P is located. A possible synoptic-scale forcing of the regional circulation was further supported by the in situ mountain breeze, usually absent at NCO-P during summer monsoon (Bonasoni et al. 2010). Lightning associated with convective storms can produce $NO_x$ (Huntrieser et al. 2002), leading to photochemical $O_3$ production in the free troposphere. To evaluate the possibility that thunderstorms occurring within the observed depression influenced the $O_3$ peak observed at NCO-P, data acquired by the Lightning Imaging Sensor (LIS) on board NASA's Tropical Rainfall Measuring Mission (TRMM) satellite were analyzed. On 22–23 September, no lightning events were observed in a range of 600 km from NCO-P, suggesting that a direct influence of lightning activity on $O_3$ levels was unlikely. The possibility that lightning occurring at more than 600 km from NCO-P could be the source of the narrow $O_3$ increase is unlikely. In fact, 1) during the event RH showed a strong decrease (if the air mass originated from the core of the depression then we would expect an RH increase) and 2) $O_3$, BC, and RH were strongly correlated, suggesting relatively low mixing of air masses that cannot support long-range transport.

### c. *Influence of ST on surface $O_3$ and BC concentrations at the NCO-P*

As suggested by the case studies in section 3b, significant variations in atmospheric composition with high $O_3$ (above 60 ppbv on average, but with peaks above 80 ppb) and low BC (mostly below 100 ng $m^{-3}$) were observed at NCO-P during ST. Such evidence suggests that, despite the significant dilution that stratospheric air masses experienced on intruding into the troposphere, ST plays an important role in determining the variability of atmospheric composition over the southern Himalaya. In general, during the identified ST, average BC and $O_3$ concentrations of 70 ± 49 ng $m^{-3}$ and 61 ± 9 ppb, respectively, were observed. Such values are notably different from average NCO-P levels (BC: 160 ± 296 ng $m^{-3}$, $O_3$: 49 ± 12 ppb), indicating that ST significantly affects $O_3$ and BC concentrations in the southern Himalaya. As already shown by Cristofanelli et al. (2010), the seasonal $O_3$ concentrations associated

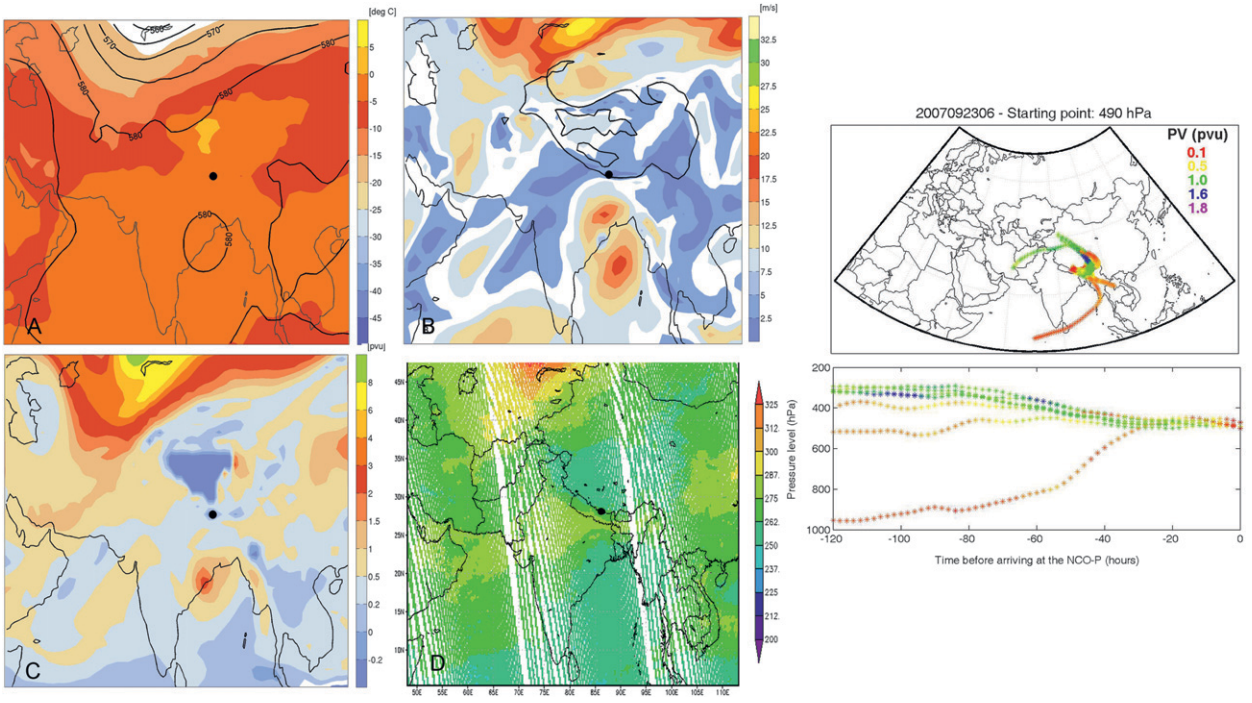


FIG. 11. As in Fig. 2, but (a) at 250 hPa and (b) at 500 hPa. Here, (a)–(c) are for 0600 UTC (1145 NPT) 23 Sep 2007, (d) is for 1200 UTC (1745 NPT) 22 Sep 2007, and the right panels are for 0600 UTC (1145 NPT) 23 Sep 2007.

with ST showed the highest values during the premonsoon (65 ± 8 ppb) and winter season (58 ± 9 ppb), with a minimum during the monsoon season (46 ± 5 ppb). As reported in Table 2, BC concentrations during ST were characterized by average values ranging from 56 ± 17 (monsoon) to 79 ± 52 (premonsoon) ng $m^{-3}$. To provide a more comprehensive description of the influence of the ST events on $O_3$ and BC at the NCO-P, on the basis of 30-min-averaged values, we calculated the differences between the average monthly means of $O_3$ ($\Delta$ozone = $O_3^{ST} - O_3^{tropo}$) and BC ($\Delta$BC = $BC^{ST} - BC^{tropo}$) during ST events ($O_3^{ST}$; $BC^{ST}$) and during "pure" tropospheric conditions ($O_3^{tropo}$; $BC^{tropo}$). On average (see Fig. 13), for all of the considered months, $\Delta$ozone showed positive values ranging from 4 (in December) up to 13 (in August and November) ppb. In general, excluding August for which the low number of detected events prevents any robust conclusion, the

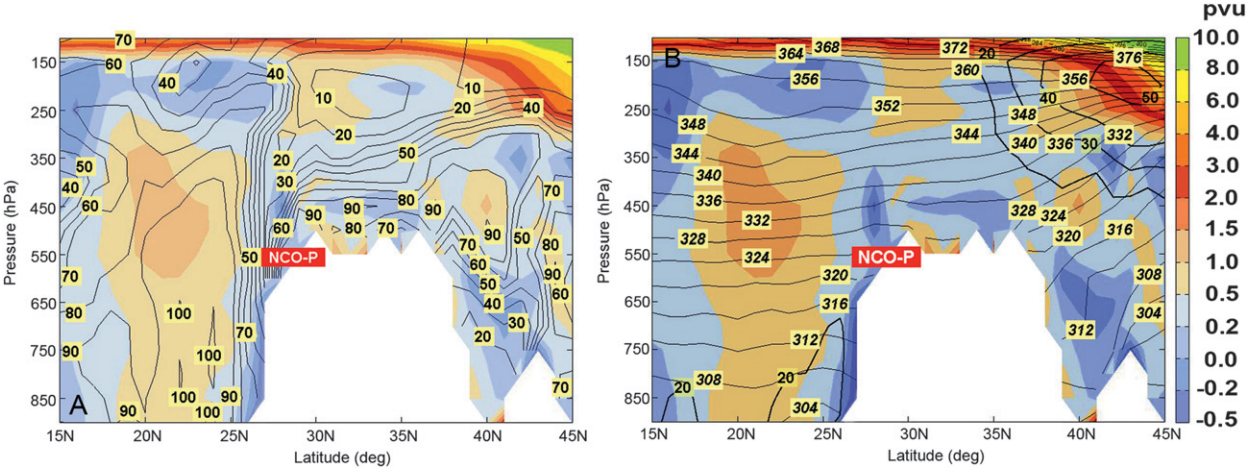


FIG. 12. As in Fig. 3, but at 0000 UTC (0545 NPT) 23 Sep 2007.

TABLE 2. For each season, for all of the 2-yr period and for the synoptic-scale scenarios defined in section 3: average BC concentration ± expanded uncertainties ($p < 0.05$) of the mean (ng $m^{-3}$) and percentage BC increase with respect to the average mean values (%).

| | All cases | | PVS | | SJS | | QSR | | MD | |
|---|---|---|---|---|---|---|---|---|---|---|
| Period | ng $m^{-3}$ | % | ng $m^{-3}$ | % | ng $m^{-3}$ | % | ng $m^{-3}$ | % | ng $m^{-3}$ | % |
| Premonsoon | 79 ± 3 | −79% | 95 ± 19 | −73% | 59 ± 8 | −83% | 91 ± 14 | −75% | — | — |
| Monsoon | 56 ± 8 | +8% | — | — | — | — | — | — | 56 ± 19 | +8% |
| Postmonsoon | 72 ± 4 | −50% | 85 ± 34 | −41% | 57 ± 11 | −60% | 78 ± 28 | −46% | — | — |
| Winter | 60 ± 3 | −56% | 54 ± 10 | −60% | 62 ± 10 | −54% | — | — | — | — |
| 2 yr | 70 ± 2 | −56% | 80 ± 13 | −51% | 60 ± 6 | −63% | 85 ± 15 | −48% | 57 ± 19 | −66% |

highest contribution of the ST events to $O_3$ at the NCO-P was observed during October–November and February–April, which spanned the postmonsoon, winter, and premonsoon seasons.

For BC, the occurrence of ST events leads to a dramatic BC decrease in March–April (ΔBC down to −360 ng $m^{-3}$), when significant transport of pollution rich in BC from the ABC can affect the measurement site during pure tropospheric periods (Bonasoni et al. 2010; Marinoni et al. 2010). During the remaining months (except August and September), the calculated ΔBC was relatively constant and ranged from −65 to −140 ng $m^{-3}$.

The BC and $O_3$ data recorded at NCO-P during ST were then analyzed as a function of the identified synoptic scenarios (Tables 2 and 3). On a seasonal basis, depending on the different synoptic-scale scenarios, average $\Delta O_3$ (i.e., the $O_3$ increase with respect to the seasonal average value) ranged from +24% (for SJS scenarios during postmonsoon) to +18% (for MD scenarios during the monsoon). For the postmonsoon, this suggests that, despite the relatively low frequency of ST (Table 1), such phenomena are particularly effective in influencing $O_3$ levels at NCO-P during this season, in agreement with the presence of a strong westerly jet stream over the southern Himalaya (Schiemann et al. 2009). The highest average $O_3$ concentrations (61 ± 9 ppbv) were observed for ST during the premonsoon season. In particular, during this season, high $O_3$ values were observed in connection with PVS (average $O_3$: 69 ± 7 ppbv) and QSR (average $O_3$: 68 ± 6 ppbv) scenarios. This is true also over the entire period of study (Table 3). Over the 2-yr period, the PVS scenario was characterized by statistically significantly (at the 90% confidence level) higher $O_3$ concentrations than was the SJS. In agreement with Sprenger et al. (2007), it can therefore be confirmed that over South Asia, ST connected with meridionally perturbed atmospheric flows are more effective in favoring deep stratospheric airmass transport than those related to well-defined "zonal" SJS.

The largest BC variation (−79%) was observed with ST during the premonsoon season, suggesting that in this season ST can have an important effect on the Himalayan atmosphere by transporting air masses that are less rich in BC and/or by suppressing up-valley flow of polluted air masses [see section 3b(3)]. With the purpose of specifically evaluating the possibility that the synoptic-scale forcing could lead to a temporary suppression of the thermal circulation along the Khumbu Valley, we analyzed the wind steadiness as defined by Singer (1967). This parameter was already applied by Henne et al. (2008) to select days affected (or not affected) by thermal wind circulation in mountain regions. As indicated by these authors, wind steadiness of greater than 0.8 in a 24-h reference period would indicate the absence of thermal wind development. As resulting by this analysis, only 19% of ST days were characterized by absence of the

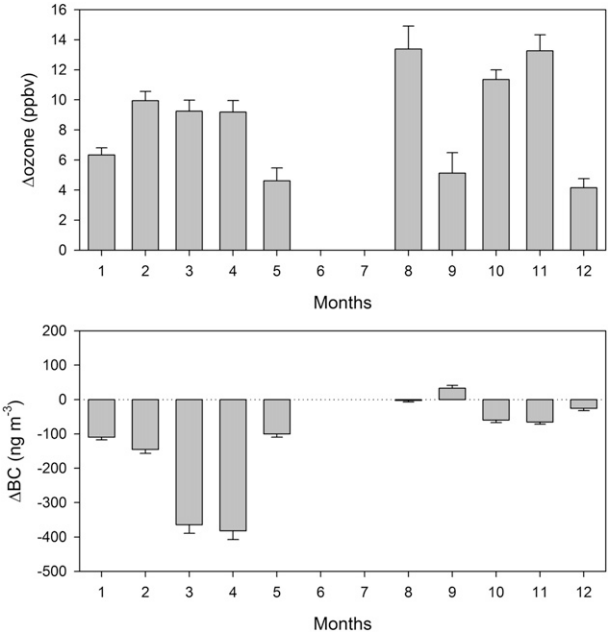


FIG. 13. Differences of monthly average values of (top) ozone (Δozone) and (bottom) black carbon (ΔBC) at NCO-P during the detected ST events and during pure tropospheric periods. The error bars denote the expanded uncertainties (significance $p < 0.05$) of the average differences.

TABLE 3. As in Table 2 but for $O_3$ (ppbv).

| Period | All cases | | PVS | | SJS | | QSR | | MD | |
|---|---|---|---|---|---|---|---|---|---|---|
| | ppbv | % | ppbv | % | ppbv | % | ppbv | % | ppbv | % |
| Premonsoon | 65 ± 1 | +9% | 69 ± 3 | +14% | 63 ± 3 | +6% | 68 ± 5 | +12% | — | — |
| Monsoon | 46 ± 1 | +18% | — | — | — | — | — | — | 46 ± 1 | +15% |
| Postmonsoon | 55 ± 1 | +22% | 54 ± 3 | +20% | 56 ± 2 | +24% | 52 ± 3 | +15% | — | — |
| Winter | 58 ± 1 | +17% | 59 ± 5 | +19% | 60 ± 3 | +20% | — | — | — | — |
| 2 yr | 61 ± 1 | +24% | 64 ± 3 | +34% | 60 ± 3 | +26% | 62 ± 6 | +29% | 46 ± 1 | −6% |

typical wind diurnal cycle at NCO-P (as observed on 27–28 April 2006). The lowest average BC values were recorded for PVS scenarios during winter (54 ± 16 ng $m^{-3}$), when significant $O_3$ increases (+19%) were also observed at NCO-P. Thus, winter ST were particularly effective in transporting stratospheric air masses down to the middle troposphere, as also suggested by James et al. (2003). As already pointed out for the monthly analysis reported in Fig. 9, only during the summer monsoon, when efficient wet scavenging typically leads to very low BC concentrations at NCO-P (Marinoni et al. 2010), BC slightly increased during ST (Table 2), probably because of the occurrences of drier air masses less impacted by wet scavenging processes. If the 2-yr period is considered and excluding the summer monsoon, the lowest BC concentrations were observed in connection with SJS scenarios (60 ± 20 ng $m^{-3}$; ΔBC: −63%). Here it can be hypothesized that the zonal atmospheric transport usually associated with such synoptic scenarios [air masses subsiding during long-range transport along the SJS; see section 3b(2) and Fig. 5] can lower the likelihood of efficient mixing with air masses from the lower troposphere, thus drastically reducing possible contamination by air masses that are rich in BC emitted at Earth's surface.

## 4. Discussion and conclusions

The work has identified and described the main synoptic scenarios characterizing ST detected at NCO-P (5079 m MSL; in the Himalaya), during the period March 2006–February 2008. Use was made of ECMWF meteorological field analyses, LAGRANTO back trajectories, and TCO fields by OMI to describe the synoptic-scale meteorological conditions that characterize the 98 ST days identified by Cristofanelli et al. (2010) during the investigated period. In particular, the presence of 1) stratospheric PV structures with a nonzonal jet stream, 2) a zonal subtropical jet stream, 3) quasi-stationary ridges, and 4) monsoon depressions were able to explain 94% of the detected ST events. A notable fraction of the events (19% of days) were related to STE occurring far upstream of the southern Himalaya, indicating that long-distance transport can be responsible for the presence of stratospheric air masses at the measurement site. This analysis relied on the events that were ''caught'' at NCO-P: here the authors argued that irreversible mixing between stratospheric and tropospheric air was likely. Because of the absence of ozone/radio soundings over the southern Himalaya it was not possible to evaluate how deeply the detected events intruded farther into the troposphere. As already reported by Cristofanelli et al. (2010), the seasonal frequency of ST at NCO-P was characterized by a clear seasonal cycle with highest values during the winter and premonsoon (23% and 22%, respectively) and the lowest values during the summer monsoon (1%). Our ST seasonal frequency appears to be in good qualitative agreement with the analyses performed by Sprenger et al. (2003), which showed the probability of tropopause folding occurrence over the global domain. Over the Himalaya, these authors reported a seasonal frequency with maxima of about 10%–15% (2%–4%) during winter and about 0% during summer for shallow (medium) tropopause folding. Note that, according to Sprenger et al. (2003), in the subtropics 50%–70% of stratosphere-to-troposphere transport is occurring in the proximity of a tropopause folding.

On an annual basis, the SJS and PVS scenarios were the most frequent (48.4% and 30.5% of ST days, respectively) and the MD class (3.1%) occurred only during the monsoon season; because of the low occurrence of observed cases, the discussion on MD scenarios can be considered only informative in this paper. On a seasonal basis the dominant synoptic-scale scenarios were PVS and SJS for the premonsoon, MD for the summer monsoon, and SJS for the winter. No clear dominant scenario was evident for the postmonsoon when the numbers of ST events related to PVS, SJS, and QSR were almost equivalent. This shows very clearly that the jet stream is the key player triggering the occurrence of ST over the southern Himalaya, both during the SJS scenario (characterized by a narrow zonal flow) and during the PVS scenario (embedded in synoptic-scale disturbances and characterized by significant meridional excursions).

The highest occurrence (4.9%) of QSR scenarios was observed during the postmonsoon season. Note that 4% of ST detected at NCO-P cannot be clearly related to the synoptic-scale scenarios listed above. The NCO-P area is characterized by very complex topography, which significantly interacts with the synoptic circulation. Several studies (e.g., Schuepbach et al. 1999; Zachariasse et al. 2000; Ding and Wang 2006; Zhu et al. 2006) have stressed the importance of ''subsynoptic'' processes (e.g., clear-air turbulence, high-mountain circulation) in favoring the descent of stratospheric air masses down to the middle troposphere. Thus, even if it cannot be completely ruled out that these few events could be related to transport from the upper troposphere, it is likely that parts of the unrecognized events are related to subsynoptic processes. Also, considering the strong interaction between synoptic-scale and smaller-scale circulations, further work is required to better address and model the role of mesoscale processes in determining the descent of stratospheric-influenced air masses to the southern Himalaya.

The paper provides four ''textbook episodes'' of deep ST occurring at NCO-P, revealed by continuous in situ analyses of meteorological parameters (AP and RH), surface $O_3$, and BC. Besides stressing the importance of continuous atmospheric observations for investigating airmass transport processes, the case studies clearly indicated that ST are important processes in determining the variability of $O_3$ and BC over the southern Himalaya, particularly during nonmonsoon seasons. During the identified ST, an average $O_3$ concentration of $61 \pm 4$ ppbv was recorded, corresponding to a +24% increase on the 2-yr average value. On a seasonal basis, the highest $\Delta O_3$ (+24%) was detected in connection with SJS scenarios during the postmonsoon and the highest $O_3$ concentrations ($69 \pm 7$ ppb) coincided with PVS scenarios during the premonsoon. During the identified ST, an average BC concentration of $70 \pm 49$ ng m$^{-3}$ was recorded, equal to less than 50% of the average BC concentration recorded at NCO-P ($160 \pm 296$ ng m$^{-3}$). The lowest $\Delta$BC (−83%) were related to SJS scenarios during the premonsoon, and the lowest BC average concentration ($54 \pm 16$ ng m$^{-3}$) was recorded for PVS scenarios during winter. As reported by Marinoni et al. (2010), the detection limit of the MAAP working at NCO-P is 11.6 ng m$^{-3}$. Thus, the average BC values presented here should be considered to be an upper estimate of the BC concentrations affecting NCO-P during ST events.

Despite the different sampling regions, the BC values observed at NCO-P during ST events appear to be comparable to the light-absorbing particle observations carried out by Baumgardner et al. (2004) within the Arctic lower stratosphere, showing average mass concentrations ranging approximately from 0.2 to 200 ng m$^{-3}$. Vertical BC profiles over the United States pointed out BC concentrations ranging from about 3 ng m$^{-3}$ in the middle troposphere (500 hPa) to 0.2–0.3 ng m$^{-3}$ in the stratosphere (Schwarz et al. 2006). Moreover, the BC values observed at NCO-P during ST events were higher than concentrations observed at other remote sites (e.g., Antarctica and the Pacific Ocean; see Bodhaine 1995). Although contributions from biomass burning and urban combustion as sources of stratospheric aerosols cannot be ruled out (e.g., Cooke and Wilson 1996; Baumgardner et al. 2004), this probably indicates that mixing with polluted tropospheric air was likely during the downward transport to the southern Himalaya. This would also imply that $O_3$ levels observed at NCO-P during the investigated ST could be partially affected by the possible influence of photochemistry during the transport. At this stage is not possible to infer an estimate of this contribution. Even if they are higher than previous observations from experimental campaigns in the middle troposphere or stratosphere, however, the observed BC concentrations during ST at NCO-P are, by far, low. This suggests that the possible contribution of photochemical $O_3$ production from mixing with polluted air masses can be relatively low. Over the investigated 2-yr period, the identified ST accounted for 12% of the ''background condition'' periods defined by Marinoni et al. (2010) for BC at NCO-P. The value increased to 25% when only nonmonsoon seasons were considered, indicating that ST plays an important role in favoring the occurrence of BC ''background'' values over the southern Himalaya from postmonsoon to premonsoon seasons. This suggests that, as well as the $O_3$ levels, ST events can significantly affect particle optical properties in the southern Himalaya, thus modifying the perturbation of the solar and infrared radiation fluxes that is due to the presence of high amounts of BC in the troposphere (Ramanathan and Carmichael 2008).

*Acknowledgments.* This study was carried out within the framework of the Ev-K2-CNR Project in collaboration with the Nepal Academy of Science and Technology, as overseen by the Memorandum of Understanding between Nepal and Italy, and with contributions from the National Research Council of Italy and the Italian Ministry of Foreign Affairs. The TCO–OMI and LIS–TRMM analyses and visualizations used in the paper were produced with the Giovanni online data system, developed and maintained by the NASA Goddard Earth Sciences (GES) Data and Information Services Center (DISC). OMI mission scientists and associated KNMI and NASA personnel are acknowledged for the production of the

data used in this research effort. The authors especially thank the Nepalese staff working at NCO-P for their valuable work under very difficult conditions.

## REFERENCES


Appenzeller, C., and J. R. Holton, 1997: Tracer lamination in the stratosphere: A global climatology. *J. Geophys. Res.,* **102,** 13 555–13 569.

——, H. C. Davies, and W. A. Norton, 1996: Fragmentation of stratospheric intrusions. *J. Geophys. Res.,* **101,** 1435–1456.

Barros, A. P., and T. J. Lang, 2003: Monitoring the monsoon in the Himalayas: Observations in central Nepal, June 2001. *Mon. Wea. Rev.,* **131,** 1408–1427.

Baumgardner, D., G. Kok, and G. Raga, 2004: Warming of the Arctic lower stratosphere by light absorbing particles. *Geophys. Res. Lett.,* **31,** L06117, doi:10.1029/2003GL018883.

Beekmann, M., and Coauthors, 1997: Regional and global tropopause fold occurrence and related ozone flux across the tropopause. *J. Atmos. Chem.,* **28,** 29–44.

Bodhaine, B. A., 1995: Aerosol absorption measurements at Barrow, Mauna Loa, and South Pole. *J. Geophys. Res.,* **100,** 8967–8975.

Böhmer, J., 2006: General climatic controls and topoclimatic variations in central and high Asia. *Boreas,* **35,** 279–294.

Bonasoni, P., and Coauthors, 2010: Atmospheric brown clouds in the Himalayas: First two years of continuous observations at the Nepal Climate Observatory-Pyramid (5079 m). *Atmos. Chem. Phys.,* **10,** 7515–7531.

Cooke, W. F., and J. J. N. Wilson, 1996: A global black carbon aerosol model. *J. Geophys. Res.,* **101,** 19 395–19 409.

Cristofanelli, P., and Coauthors, 2009: Influence of lower stratosphere/upper troposphere (LS/UT) transport events on surface ozone at the Everest-Pyramid GAW Station (Nepal, 5079 m a.s.l.): First year of analysis. *Int. J. Remote Sens.,* **30,** 4083–4097.

——, and Coauthors, 2010: Tropospheric ozone variations at the Nepal Climate Observatory-Pyramid (Himalayas, 5079 m a.s.l.) and influence of deep stratospheric intrusion events. *Atmos. Chem. Phys.,* **10,** 6537–6549.

Croci-Maspoli, M., C. Schwierz, and H. C. Davies, 2007: A multifaceted climatology of atmospheric blocking and its recent linear trend. *J. Climate,* **20,** 633–649.

Danielsen, E. F., 1968: Stratospheric-tropospheric exchange based on radioactivity, ozone and potential vorticity. *J. Atmos. Sci.,* **25,** 502–518.

Das, S. S., 2009: A new perspective on MST radar observations of stratospheric intrusions into troposphere associated with tropical cyclone. *Geophys. Res. Lett.,* **36,** L15821, doi:10.1029/2009GL039184.

Davies, T. D., and E. Schuepbach, 1994: Episodes of high ozone concentrations at the earth's surface resulting from transport down from the upper troposphere/lower stratosphere. *Atmos. Environ.,* **28,** 53–68.

Ding, D., and T. Wang, 2006: Influence of stratosphere-to-troposphere exchange on the seasonal cycle of surface ozone at Mount Waliguan in western China. *Geophys. Res. Lett.,* **33,** L03803, doi:10.1029/2005GL024760.

Ebel, A., H. Feldmann, H. J. Jakobs, M. Memmesheimer, D. Offermann, V. Kuell, B. Schäler, 2008: Simulation of transport and composition changes during a blocking episode over the east Atlantic and north Europe. *Ecol. Modell.,* **217** (3–4), 240–254.

Ellrod, G. P., and D. L. Knapp, 1992: An objective clear-air turbulence forecasting technique: Verification and operational use. *Wea. Forecasting,* **7,** 150–165.

Flanner, M. G., C. S. Zender, P. G. Hess, N. M. Mahowald, T. H. Painter, V. Ramanathan, and P. J. Rasch, 2009: Springtime warming and reduced snow cover from carbonaceous particles. *Atmos. Chem. Phys.,* **9,** 2481–2497.

Forster, P., and Coauthors, 2007: Changes in atmospheric constituents and in radiative forcing. *Climate Change 2007: The Physical Science Basis,* S. Solomon et al., Eds., Cambridge University Press, 129–234.

Gauss, M., and Coauthors, 2003: Radiative forcing in the 21st century due to ozone changes in the troposphere and the lower stratosphere. *J. Geophys. Res.,* **108,** 4292, doi:10.1029/2002JD002624.

GAW, 1992: Report of the WMO meeting of experts on the quality assurance plan for the GAW, Garmisch-Partenkirchen, Germany, 28-30 March 1992. WMO Tech. Doc. 513, 84 pp.

Goering, M. A., W. A. Gallus Jr., M. A. Olsen, and J. L. Stanford, 2001: Role of stratospheric air in a severe weather event: Analysis of potential vorticity and ozone. *J. Geophys. Res.,* **106,** 11 813–11 823.

Henne, S., J. Klausen, W. Junkermann, J. M. Kariuki, J. O. Aseyo, and B. Buchmann, 2008: Representativeness and climatology of carbon monoxide and ozone at the global GAW station Mt. Kenya in equatorial Africa. *Atmos. Chem. Phys.,* **8,** 3119–3139.

Hitchman, M. H., M. L. Buker, G. J. Tripoli, R. B. Pierce, J. A. Al-Saadi, E. V. Browell, and M. A. Avery, 2004: A modeling study of an east Asian convective complex during March 2001. *J. Geophys. Res.,* **109,** D15S14, doi:10.1029/2003JD004312.

Holton, J. R., P. H. Haynes, M. E. McIntyre, A. R. Douglass, R. B. Rood, and L. Pfister, 1995: Stratosphere–troposphere exchange. *Rev. Geophys.,* **33,** 403–439.

Hoskins, B. J., M. E. McIntyre, and A. W. Robertson, 1985: On the use and significance of isentropic potential vorticity maps. *Quart. J. Roy. Meteor. Soc.,* **111,** 877–946.

Hudson, R. G., A. D. Frolov, M. F. Andrade, and M. B. Follette, 2003: The total ozone field separated into meteorological regimes. Part I: Defining the regimes. *J. Atmos. Sci.,* **60,** 1669–1677.

Huntrieser, H., and Coauthors, 2002: Airborne measurements of NOx, tracer species, and small particles during the European Lightning Nitrogen Oxides Experiment. *J. Geophys. Res.,* **107,** 4113, doi:10.1029/2000JD000209.

Jacobson, M. Z., 2002: *Atmospheric Pollution: History, Science and Regulation.* Cambridge University Press, 399 pp.

James, P., A. Stohl, C. Forster, S. Eckhardt, P. Seibert, and A. Frank, 2003: A 15-year climatology of stratosphere–troposphere exchange with a Lagrangian particle dispersion model 2. Mean climate and seasonal variability. *J. Geophys. Res.,* **108,** 8522, doi:10.1029/2002JD002639.

Keyser, D., and M. A. Shapiro, 1986: A review of the structure and dynamics of upper-level frontal zones. *Mon. Wea. Rev.,* **114,** 452–499.

Kopacz, M., D. L. Mauzerall, J. Wang, E. M. Leibensperger, D. K. Henze, and K. Singh, 2011: Origin and radiative forcing of black carbon transported to the Himalayas and Tibetan Plateau. *Atmos. Chem. Phys.,* **11,** 2837–2852.

Kumar, K. K., 2006: VHF radar observations of convectively generated gravity waves: Some new insights. *Geophys. Res. Lett.,* **33,** L01815, doi:10.1029/2005GL024109.

Langford, A. O., 1999: Stratosphere–troposphere exchange at the subtropical jet: Contribution to the tropospheric ozone budget at midlatitudes. *Geophys. Res. Lett.,* **26,** 2449–2452.

Lelieveld, J., and F. J. Dentener, 2000: What controls tropospheric ozone? *J. Geophys. Res.,* **105,** 3531–3551.

Levelt, P. F., and Coauthors, 2006a: The Ozone Monitoring Instrument. *IEEE Trans. Geosci. Remote Sens.,* **44,** 1093–1101.

——, E. Hilsenrath, G. W. Leppelmeier, G. H. J. van Den Oord, P. K. Bhartia, J. Tamminen, J. F. de Haan, and J. P. Veefkind, 2006b: Science objectives of the Ozone Monitoring Instrument. *IEEE Trans. Geosci. Remote Sens.,* **44,** 1199–1208.

Loring, R. O. J., H. E. Fuelberg, J. Fishman, M. V. Watson, and E. V. Browell, 1996: Influence of a middle-latitude cyclone on tropospheric ozone distributions during a period of TRACE A. *J. Geophys. Res.,* **101,** 23 941–23 956.

Marinoni, A., and Coauthors, 2010: Aerosol mass and black carbon concentrations, a two year record at NCO-P (5079 m, Southern Himalayas). *Atmos. Chem. Phys.,* **10,** 8551–8562.

Menon, S., D. Koch, G. Beig, S. Sahu, J. Fasullo, and D. Orlikowski, 2010: Black carbon aerosols and the third polar ice cap. *Atmos. Chem. Phys.,* **10,** 4559–4571.

Mohanakumar, K., 2008: *Stratosphere Troposphere Interactions: An Introduction.* Springer, 416 pp.

Moore, J. T., and G. E. Vanknowe, 1992: The effect of jet-streak curvature on kinematic fields. *Mon. Wea. Rev.,* **120,** 2429–2441.

Nieto, R., M. Sprenger, H. Wernli, R. M. Trigo, and L. Gimeno, 2008: Identification and climatology of cut-off lows near the tropopause. *Ann. N. Y. Acad. Sci.,* **1146,** 256–290.

Ordóñez, C., H. Mathis, M. Furger, S. Henne, C. Hüglin, J. Staehelin, and A. S. H. Prévôt, 2005: Changes of daily surface ozone maxima in Switzerland in all seasons from 1992 to 2002 and discussion of summer 2003. *Atmos. Chem. Phys.,* **5,** 1187–1203.

Palazzi, E., and Coauthors, 2009: Diagnostics of the tropical tropopause layer from in-situ observations and CCM data. *Atmos. Chem. Phys.,* **9,** 9349–9367.

Palmen, E., and C. W. Newton, 1969: *Atmospheric Circulation Systems: Their Structure and Physical Interpretation.* Academic Press, 603 pp.

Panday, A. K., and R. G. Prinn, 2009: Diurnal cycle of air pollution in the Kathmandu Valley, Nepal: Observations. *J. Geophys. Res.,* **114,** D09305, doi:10.1029/2008JD009777.

Ramanathan, V., and G. Carmichael, 2008: Global and regional climate changes due to black carbon. *Nat. Geosci.,* **1,** 221–227, doi:10.1038/ngeo156.

——, and Coauthors, 2007: Atmospheric brown clouds: Hemispherical and regional variations in long-range transport, absorption, and radiative forcing. *J. Geophys. Res.,* **112,** D22S21, doi:10.1029/2006JD008124.

——, and Coauthors, 2008: Atmospheric brown clouds: Regional assessment report with focus on Asia. United Nations Environment Programme Rep., 354 pp. [Available online at http://www.rrcap.unep.org/abc/impact/.]

Schiemann, R., D. Lüthi, and C. Schär, 2009: Seasonality and interannual variability of the westerly jet in the Tibetan Plateau region. *J. Climate,* **22,** 2940–2957.

Schoeberl, M. R., and Coauthors, 2006: Overview of the EOS-*Aura* mission. *IEEE Trans. Geosci. Remote Sens.,* **44,** 1066–1074, doi:10.1109/TGRS.2005.861950.

Schuepbach, E., T. D. Davies, and A. C. Massacand, 1999: An unusual springtime ozone episode at high elevation in the Swiss Alps: Contributions both from cross-tropopause exchange and from the boundary layer. *Atmos. Environ.,* **33,** 1735–1744.

Schwarz, J. P., and Coauthors, 2006: Single-particle measurements of midlatitude black carbon and light-scattering aerosols from the boundary layer to the lower stratosphere. *J. Geophys. Res.,* **111,** D16207, doi:10.1029/2006JD007076.

Shapiro, M. A., T. Hampel, and A. J. Krueger, 1987: The Arctic tropopause fold. *Mon. Wea. Rev.,* **115,** 444–454.

Singer, I. A., 1967: Steadiness of the wind. *J. Appl. Meteor.,* **6,** 1033–1038.

Sprenger, M., and H. Wernli, 2003: A Northern Hemispheric climatology of cross-tropopause exchange for the ERA15 time period (1979–1993). *J. Geophys. Res.,* **108,** 8521, doi:10.1029/2002JD002636.

——, M. Croci-Maspoli, and H. Wernli, 2003: Tropopause folds and cross-tropopause exchange: A global investigation based upon ECMWF analyses for the time period March 2000 to February 2001. *J. Geophys. Res.,* **108,** 8518, doi:10.1029/2002JD002587.

——, H. Wernli, and M. Bourqui, 2007: Stratosphere–troposphere exchange and its relation to potential vorticity streamers and cutoffs near the extratropical tropopause. *J. Atmos. Sci.,* **64,** 1587–1602.

Sudo, K., Y. Masaaki, and H. Akimoto, 2003: Future changes in stratosphere–troposphere exchange and their impacts on future tropospheric ozone simulations. *Geophys. Res. Lett.,* **30,** 2256, doi:10.1029/2003GL018526.

Traub, M., and J. Lelieveld, 2003: Cross-tropopause transport over the eastern Mediterranean. *J. Geophys. Res.,* **108,** 4712, doi:10.1029/2003JD003754.

Trickl, T., H. Feldmann, H.-J. Kanter, H.-E. Scheel, M. Sprenger, A. Stohl, and H. Wernli, 2010: Forecasted deep stratospheric intrusions over central Europe: Case studies and climatologies. *Atmos. Chem. Phys.,* **10,** 499–524.

——, N. Bärtsch-Ritter, H. Eisele, M. Furger, R. Mücke, M. Sprenger, and A. Stohl, 2011: High-ozone layers in the middle and upper troposphere above central Europe: Potential import from the stratosphere along the subtropical jet stream. *Atmos. Chem. Phys. Discuss.,* **11,** 9343–9366.

Vaughan, G., and J. D. Price, 1989: Ozone transport into the troposphere in a cut-off low event. *Ozone in the Atmosphere,* R. D. Bojkov and P. Fabian, Eds., Deepak, 415–416.

Wernli, H., and H. Davies, 1997: A Lagrangian-based analysis of extratropical cyclones. Part I: The method and some applications. *Quart. J. Roy. Meteor. Soc.,* **123,** 467–489.

Wild, O., 2007: Modelling the global tropospheric ozone budget: Exploring the variability in current models. *Atmos. Chem. Phys.,* **7,** 2643–2660.

Wimmers, A. J., and J. L. Moody, 2004: Tropopause folding at satellite-observed spatial gradients: 1. Verification of an empirical relationship. *J. Geophys. Res.,* **109,** D19306, doi:10.1029/2003JD004145.

Yasunari, T. J., and Coauthors, 2010: Estimated impact of black carbon deposition during pre-monsoon season from Nepal Climate Observatory–Pyramid data and snow albedo changes over Himalayan glaciers. *Atmos. Chem. Phys.,* **10,** 6603–6615.

Zachariasse, M., P. F. J. van Velthoven, H. G. J. Smit, J. Lelieveld, T. K. Mandal, and H. Kelder, 2000: Influence of stratosphere-troposphere exchange on tropospheric ozone over the tropical Indian Ocean during the winter monsoon. *J. Geophys. Res.,* **105,** 15 403–15 416.

Zhu, T., W. Lin, Y. Song, X. Cai, H. Zou, L. Kang, L. Zhou, and H. Akimoto, 2006: Downward transport of ozone-rich air near Mt. Everest. *Geophys. Res. Lett.,* **33,** L23809, doi:10.1029/2006GL027726.